Four-bar mechanism's PD and neural adaptive control for the thorax of the micromechanical flying insects

Romulus Lungu
University of Craiova, Electrical, Energetic, and Aerospatiale Engineering Department
107 Decebal Street, 200440 Craiova, Romania
romulus_lungu@yahoo.com

Lucian Sepcu
University of Craiova, Electrical, Energetic, and Aerospatiale Engineering Department
107 Decebal Street, 200440 Craiova, Romania
lsepcu@elth.ucv.ro

Mihai Lungu[1]
University of Craiova, Electrical, Energetic, and Aerospatiale Engineering Department
107 Decebal Street, 200440 Craiova, Romania
Lma1312@yahoo.com

ABSTRACT

The paper focuses on the dynamics and control of the non-deformable and deformable four-bar mechanism (three of the bars are mobile and one is fixed), this being a subsystem of the micromechanical flying insects' thorax. The control of the mechanism (six order system described by Lagrange equations) is initially achieved by using a proportional-derivative control law, a Newton-Raphson type algorithm, and the Lyapunov theory. Because the thorax's dynamics is strongly nonlinear and is characterized by fast time varying coefficients, the PD control law cannot always guarantee small overshoot and angular rates; to overcome this drawback, over the control law PD component we superpose a neural adaptive component which compensate the error of the global nonlinearity's approximation associated to the thorax's dynamics. The two obtained control systems are validated by complex numerical simulations.

[1] Corresponding author

INTRODUCTION

The MFI (Micromechanical Flying Insect) type servo-mechanisms (servo-systems, servo-actuators) are physical models of the insects' thorax. Such a servo-mechanism generally consists of three subsystems: the command subsystem (electric engine or piezoelectric actuator), the wing actuation equipment (the cinematic mechanism), and the controller. The most used command subsystems (equipment) are the piezoelectric actuators; these work together with mechanical transmission elements for the wing's actuation, e.g. the four-bar mechanism [1-11]. In recent years, the studies and researches have been developed and culminated in the development of efficient flying robots [2, 12-16], but, from our information, none of them has used both the dynamic inversion and forward neural networks in the design of the MFIs' control; this is achieved in this paper, being interesting to see if such a control law can guarantee the control of the four-bar mechanism of the MFIs. Thus, our aim is to design new control systems for the control of the four-bar mechanism (subsystem of the micromechanical flying insects' thorax); before the design process, we obtain the mathematical model (dynamics) of the four-bar mechanism by means of the Lagrange equations [17]. It will be shown that the dynamics of the four-bar mechanism is described by a nonlinear system having three equations which depend on three variables (the rotation angles of the mobile bars); one of the three variables (the rotation angle of the driving bar) is independent, while the other two are dependent on the first one. The states depending on the independent variable are calculated by using a Newton-Raphson type algorithm [18]. To obtain the parameters of the proportional-derivative control law, the Lyapunov theory is used; it will be shown that the dynamics of the servo-actuators is nonlinear and has fast time varying coefficients, and, therefore, if the PD control laws lead to dynamic processes characterized by high overshoot and angular rates, the deformation and even damage of the four-bar mechanism may occur. As a consequence, from some points of view, a neural adaptive control which compensates the global nonlinearity would be a better choice. In the design of the neural adaptive control law, we use the dynamic inversion technique and neural networks. The adaptive control law has two components: the role of the first one is to compensate the global nonlinearities (compensation of the dynamic inversion error), while the second one is useful for the control of the linear subsystem with respect to the driving bar angle [19-23].

The paper is organized as follows: the dynamics of the four-bar mechanism together with the calculation of the two dependent variables is presented in the second section; the design of the two control laws (proportional-derivative and adaptive) for the MFI's control is presented in the third section; in the fourth section of the paper, complex simulations to validate the proposed automatic control systems have been performed and analyzed; finally, some conclusions are shared in the fifth section.

DYNAMIC MODEL OF THE FOUR-BAR MECHANISM

Conventional rigid body four-bar mechanism

The four-bar mechanism is a subsystem of a MFI's thorax. The four-bar mechanism has three mobile bars (all considered to be rigid). The structure of such mechanism is presented in Fig. 1; each of the three mobile bars is considered rigid [10]; the only fixed bar is denoted in Fig. 1 with *AD*; $\vec{r}_i, i=\overline{1,3}$ are the position vectors associated to the mobile bars' mass centers (the bars have the masses m_i), $\vec{l}_i, i=\overline{1,4}$ are the position vectors associated to the joint *B* with respect to *A*, joint *C* with respect to *B*, joint *D* with respect to *C*, and joint *D* with respect to *A*; $\delta_i, i=\overline{1,3}$ express the angular positions of the $\vec{r}_i$ with respect to the position vectors $\vec{l}_i$; $\theta_i, i=\overline{1,4}$, are the angular positions of $\vec{l}_i$ with respect to the reference axis *Ox* of the coordinate system *Oxy*. The coordinates of the mobile bars' mass centers with respect to the *Oxy* reference system are x_i, y_i. The local coordinates' systems $A\xi_1\eta_1, B\xi_2\eta_2, D\xi_3\eta_3$ are connected to the mobile bars. The Cartesian coordinates of the mobile bars' mass centers can be expressed as functions of following angular coordinates:

$$\begin{aligned}
&x_1(\theta_1)=r_1\cos(\theta_1+\delta_1), y_1(\theta_1)=r_1\sin(\theta_1+\delta_1),\\
&x_2(\theta_1,\theta_2)=l_1\cos(\theta_1)+r_2\cos(\theta_2+\delta_2), y_2(\theta_1,\theta_2)=l_1\sin(\theta_1)+r_2\sin(\theta_2+\delta_2),\\
&x_3(\theta_3,\theta_4)=l_4\cos\theta_4+r_3\cos(\theta_3+\delta_3), y_3(\theta_3,\theta_4)=l_4\sin\theta_4+r_3\sin(\theta_3+\delta_3).
\end{aligned} \tag{1}$$

By using the previous equations, the velocities of the mobile bars' mass centers with respect to the Cartesian system (for θ_4 = constant) are obtained as following:

$$\begin{aligned}
&V_{1x}=\dot{x}_1=-r_1\dot{\theta}_1\sin(\theta_1+\delta_1), V_{1y}=r_1\dot{\theta}_1\cos(\theta_1+\delta_1); V_1=r_1\dot{\theta}_1,\\
&V_{2x}=\dot{x}_2=-\left[l_1\sin\theta_1+r_2\frac{\dot{\theta}_2}{\dot{\theta}_1}\sin(\theta_2+\delta_2)\right]\dot{\theta}_1, V_{2y}=\left[l_1\cos\theta_1+r_2\frac{\dot{\theta}_2}{\dot{\theta}_1}\cos(\theta_2+\delta_2)\right]\dot{\theta}_1,\\
&V_{3x}=\dot{x}_3=\left[-r_3\frac{\dot{\theta}_3}{\dot{\theta}_1}\sin(\theta_3+\delta_3)\right]\dot{\theta}_1, V_{3y}=\dot{y}_3=\left[r_3\frac{\dot{\theta}_3}{\dot{\theta}_1}\cos(\theta_3+\delta_3)\right]\dot{\theta}_1, V_3=r_3\dot{\theta}_3,
\end{aligned} \tag{2}$$

and $V_{ix}=u_i\dot{\theta}_1, V_{iy}=v_i\dot{\theta}_1, i=\overline{1,3}$, respectively, with

$$\begin{aligned}
&u_1=-r_1\sin(\theta_1+\delta_1), v_1=r_1\cos(\theta_1+\delta_1),\\
&u_2=-[l_1\sin\theta_1+r_2w_2\sin(\theta_2+\delta_2)], v_2=l_1\cos\theta_1+r_2w_2\cos(\theta_2+\delta_2),\\
&u_3=-r_3w_3\sin(\theta_3+\delta_3), v_3=r_3w_3\cos(\theta_3+\delta_3), w_i=\dot{\theta}_i/\dot{\theta}_1, i=\overline{1,3}.
\end{aligned} \tag{3}$$

Thus, the dynamics of the four-bar mechanism is described by three equations which are nonlinear with respect to three variables (the rotation angles of the mobile bars); one of the three variables (the rotation angle of the driving bar) is independent, while the other two are dependent on the first one. The non-dimensional variables u_i and v_i can be obtained starting from the equation which describes the connection between the four-bar, i.e. [17]: $\vec{l}_1 + \vec{l}_2 - \vec{l}_3 = \vec{l}_4$; if this equation is projected on the Cartesian system's axes, one gets:

$$l_1 \cos\theta_1 + l_2 \cos\theta_2 - l_3 \cos\theta_3 = l_4 \cos\theta_4, l_1 \sin\theta_1 + l_2 \sin\theta_2 - l_3 \sin\theta_3 = l_4 \sin\theta_4, \quad (4)$$

and, by differentiating ($\theta_4 =$ constant), respectively:

$$-\frac{l_2}{l_1}\frac{\sin\theta_2}{\sin\theta_1} w_2 + \frac{l_3}{l_1}\frac{\sin\theta_3}{\sin\theta_1} w_3 = 1, -\frac{l_2}{l_1}\frac{\cos\theta_2}{\cos\theta_1} w_2 + \frac{l_3}{l_1}\frac{\cos\theta_3}{\cos\theta_1} w_3 = 1. \quad (5)$$

The equations (4) express the fact that only the coordinate θ_1 is an independent variable, while the other two depend on this variable; $\theta_2 = \theta_2(\theta_1), \theta_3 = \theta_3(\theta_1)$. Similarly, the equations (5) express the fact that only the angular rate $\dot{\theta}_1$ is independent, while $\dot{\theta}_2$ and $\dot{\theta}_3$ depend on $\dot{\theta}_1$; now, by solving the system (5) with respect to the unknown variables $w_2 = \dot{\theta}_2 / \dot{\theta}_1$ and $w_3 = \dot{\theta}_3 / \dot{\theta}_1$, one yields:

$$w_2 = \frac{l_1}{l_2}\frac{\sin(\theta_3 - \theta_1)}{\sin(\theta_2 - \theta_3)}, w_3 = \frac{l_1}{l_3}\frac{\sin(\theta_2 - \theta_1)}{\sin(\theta_2 - \theta_3)}. \quad (6)$$

To determine the four-bar mechanism dynamical model, one uses the Lagrange equation

$$\frac{\mathrm{d}}{\mathrm{d}t}\left(\frac{\partial K}{\partial \dot{\theta}_1}\right) - \frac{\partial K}{\partial \theta_1} + \frac{\partial P}{\partial \theta_1} + \frac{\partial D}{\partial \dot{\theta}_1} = 0, \quad (7)$$

where *K* is the total kinetic energy, *P* - the potential energy, *D* - the dissipated energy; $P = P(\theta_1)$ has two components: $P_g(\theta_1) -$ the potential energy of the mechanism having non-deformable bars and $P_t(\theta_1) -$ the potential energy due to torsion,

$$P(\theta_1) = P_g(\theta_1) + P_t(\theta_1), P_g(\theta_1) = g(m_1 y_1 + m_2 y_2 + m_3 y_3), P_t(\theta_1) = -M_\theta \theta_1, \tag{8}$$

with $y_i, i = \overline{1,3}$ having the forms (1) and M_θ – the torsion moment (torque) of the bar 1.

The total kinetic energy of the four-bar mechanism has the expression [10]:

$$K = K(\theta_1, \dot{\theta}_1) = \frac{1}{2}\sum_{i=1}^{3}\left[m_i\left(V_{ix}^2 + V_{iy}^2\right) + J_i \dot{\theta}_i^2\right], \tag{9}$$

where J_i represents the inertia moment of the bar "*i*" with respect to the axis which is rectangular on the *Oxy* plane and passes through the mass center of the bar "*i*"; the components V_{ix} and V_{iy} are described by equations (2) and (3). With these, (9) becomes:

$$K = \frac{1}{2} J(\theta)\dot{\theta}^2, J(\theta) = \sum_{i=1}^{3}\left[m_i\left(u_i^2 + v_i^2\right) + J_i\right] w_i^2, \tag{10}$$

with $\theta = \theta_1$. To obtain the equivalent inertia moment $J(\theta)$, the variables $u_i, v_i, i = \overline{1,3}$ are expressed with respect to the local coordinates ξ_i, η_i as follows: $\xi_i = r_i \cos\delta_i$, $\eta_i = r_i \sin\delta_i$. With these, the variables $u_i, v_i, i = \overline{1,3}$ becomes:

$$\begin{aligned}
u_1 &= -\xi_1 \sin\theta - \eta_1 \cos\theta, v_1 = \xi_1 \cos\theta - \eta_1 \sin\theta, \\
u_2 &= [-l_1 \sin\theta + (\xi_2 \sin\theta_2 + \eta_2 \cos\theta_2)] w_2, v_2 = [l_1 \cos\theta + (\xi_2 \cos\theta_2 - \eta_2 \sin\theta_2)] w_2, \\
u_3 &= -(\xi_3 \sin\theta_3 + \eta_3 \cos\theta_3) w_2, v_3 = (\xi_3 \cos\theta_3 - \eta_3 \sin\theta_3) w_3;
\end{aligned} \tag{11}$$

replacing these forms in (10), one gets:

$$J(\theta) = C_0 + C_1 w_2^2 + C_3 w_2 \cos(\theta_2 - \theta + \delta_2), \tag{12}$$

with $C_0 = J_1 + m_1 r_1^2 + m_2 l_1^2, C_1 = J_2 + m_2 r_2^2, C_2 = J_3 + m_3 r_3^2, C_3 = 2 m_2 l_1 r_2$. Now, to calculate the second term in (7), one first calculates $\frac{\mathrm{d}J(\theta)}{\mathrm{d}\theta}$ by using (12); it results [2]:

$$\begin{aligned}
\frac{1}{2}\frac{\mathrm{d}J(\theta)}{d\theta} &= C_1 w_2 \frac{\mathrm{d}w_2}{\mathrm{d}\theta} + C_2 w_3 \frac{\mathrm{d}w_3}{\mathrm{d}\theta_1} + \\
&+ \frac{1}{4} C_3 \left[\frac{\mathrm{d}w_2}{\mathrm{d}\theta}\cos(\theta_2 - \theta + \delta_2) - w_2 \sin(\theta_2 - \theta + \delta_2) - w_2^2 \sin(\theta_2 - \theta + \delta_2)\right],
\end{aligned} \tag{13}$$

with $\frac{\mathrm{d}w_2}{\mathrm{d}\theta}=\frac{l_1}{l_2}\frac{D_1+D_2}{\sin^2(\theta_2-\theta)},\frac{\mathrm{d}w_3}{\mathrm{d}\theta}=\frac{l_1}{l_3}\frac{D_3+D_4}{\sin^2(\theta_2-\theta_3)}$, and

$$\begin{aligned}&D_1=(w_3-1)\sin(\theta_2-\theta_3)\cos(\theta_3-\theta),D_2=(w_3-w_2)\sin(\theta_3-\theta)\cos(\theta_2-\theta),\\&D_3=(w_2-1)\sin(\theta_2-\theta_3)\cos(\theta_2-\theta),D_4=(w_3-w_2)\sin(\theta_2-\theta)\cos(\theta_2-\theta_3).\end{aligned} \tag{14}$$

Taking into account equations (8) and (1), the third term in (7) becomes:

$$\frac{\partial P}{\partial\theta}=G(\theta)=G_0+G_1w_2+G_2w_3, \tag{15}$$

where $G_0=m_1gr_1\cos(\theta+\delta_1),G_1=m_2g[l_1\cos\theta+r_2\cos(\theta_2+\delta_2)],G_2=m_3gr_3\cos(\theta_3+\delta_3)$. If the dissipated energy *D* is not taken into account, the equation (7) gets the form:

$$J(\theta)\ddot{\theta}+\frac{1}{2}\frac{\mathrm{d}J(\theta)}{\mathrm{d}\theta}\dot{\theta}^2+G_0+G_1w_2+G_2w_3=M_\theta. \tag{16}$$

Four-bar mechanism having two elastic bars

The diagram of the mechanical model associated to the mechanism with four bars, taking into account the elastic deformations of the bars 1 and 3 (*AB* and *CD*), is presented in Fig. 2 [3]; in this figure, m_1^*, m_2^*, and m_3^* are the mobile bars' equivalent masses, $l_i, i=\overline{1,4}$– the lengths of the four bars which interact with the elastic and dissipative external environment (atmospheric air); the interactions are modeled by elastic and damping elements having the elasticity coefficients k_1, k_3 and the damping coefficients b_1, b_3, b_w. The geometric elements θ_i, δ_i, r_i, and l_i from Fig. 1 become here $\theta_1=\theta,\theta_2=-\phi$, $\theta_3=\psi$, $\theta_4=0$, $\delta_1=0,\delta_2=\beta,\delta_3=0,r_1=l_1,r_3=l_3$; δ_1 and δ_3 express the position of the four-bar mechanism (bars 1 and 3 are elastically deformable) with respect to the mechanism having four rigid bars. Corresponding to the displacements δ_1 and δ_3, the angular position of the mechanism with two deformable bars with respect to the one having only rigid bars is expressed by means of the angles $\tilde{\theta} = \theta - \theta_0$ and $\tilde{\psi} = \psi - \psi_0$ (θ_0 and ψ_0 are the values of the angles θ and ψ, respectively, for the mechanism having four rigid bars).

The wing of MFI is attached to the slide (bar) *FE*. The mass center of the ensemble *BC* bar – *FE* slide – wing is situated near the middle of the *FE* slide and it has the position vector r_2 ;

$$x_2 = \frac{\sum_{i=1}^{3} m_i x_i}{\sum_{i=1}^{3} m_i} = \frac{(m_2 + m_w)\frac{l_a}{2}}{m_2^*} \cong \frac{l_a}{2}, r_2 = \frac{l_2}{2\cos\beta}, \tag{17}$$

where $m_2^* = m_2 + m_\phi + m_w \cong m_2 + m_w, m_2$ is the BC bar's mass, $m_\phi -$ the FE slide's mass, and $m_w -$ the wing's mass; $\tan(\beta) \cong l_a / l_2$.

The kinetic energy *K* has expression (10), with *J*(θ) described by (12), where $J_1 = J_3 = 0; C_0 = (m_1^* + m_2^*) l_1^2, C_1 = J_2 + m_2^* r_2^2 = J_w + m_2^* \frac{l_a^2}{3}, C_2 = m_3^* l_3^2, C_3 = 2 m_2^* l_1 r_2$; the equations (6) become now:

$$w_2 = \frac{l_1}{l_2} \frac{\sin(\theta - \psi)}{\sin(\psi + \phi)}, w_3 = \frac{l_1}{l_3} \frac{\sin(\phi + \theta)}{\sin(\phi + \psi)}. \tag{18}$$

The potential energy has the form (8), i.e.:

$$P^*(\theta) = P_g^*(\theta) + P_t(\theta) = g\left(m_1^* y_1 + m_2^* y_2 + m_3^* y_3\right) + \frac{1}{2} k_1 \delta_1^2 + \frac{1}{2} k_3 \delta_3^2 - M_\theta \theta, \tag{19}$$

with $y_i, i = \overline{1,3}$ of forms (1). Using the geometric equation: $l_3 \sin\psi = l_1 \sin\theta - l_2 \sin\phi$, equation (19) becomes

$$P^*(\theta) = g\left[m_t l_1 \sin\theta + m_2^* r_2 \sin(\phi - \beta) - m_3^* l_2 \sin\phi\right] + \frac{1}{2} k_1 l_1^2 (\theta - \theta_0)^2 + \frac{1}{2} k_3 l_3^2 (\psi - \psi_0)^2, \tag{20}$$

with $m_t = m_1^* + m_2^* + m_3^*$. The dissipated energy is expressed as follows [3]:

$$D = \frac{1}{2}\left(b_1\dot{\delta}_1^2 + b_w l_a^2 \dot{\phi}^2 + b_3\dot{\delta}_3^2\right), \quad (21)$$

where $\dot{\delta}_1 = l_1\dot{\tilde{\theta}} = l_1\dot{\theta}, \dot{\delta}_3 = l_3\dot{\tilde{\psi}} = l_3\dot{\psi} = l_3 w_3\dot{\theta}, \dot{\phi} = -w_2\dot{\theta}$. Thus, one obtains:

$$D = \frac{1}{2}F(\theta)\dot{\theta}^2, F(\theta) = b_1 l_1^2 + b_w l_a^2 w_2^2 + b_3 l_3^2 w_3^2 \,. \quad (22)$$

The dynamic model of the four-bar mechanism, having two elastically deformable bars (AB and CD), described initially by the Lagrange equation (7), replacing P with P^*, is now:

$$J(\theta)\ddot{\theta} + \frac{1}{2}\frac{\mathrm{d}J(\theta)}{d\theta}\dot{\theta}^2 + G_0 + G_1 w_2 + G_2 w_3 + F(\theta)\dot{\theta} = M_\theta \,, \quad (23)$$

where $G_0 = k_1 l_1^2\tilde{\theta} + m_t g l_1 \cos\theta, G_1 = m_2^* g r_2 \cos(\phi - \beta) + m_3^* g l_2 \cos\phi, G_2 = k_3 l_3^2\tilde{\psi} = k_3 l_3^2 w_3\tilde{\theta}.$

The expression of $J(\theta)$ is (12), while the form of $\frac{1}{2}\frac{\mathrm{d}J(\theta)}{\mathrm{d}\theta}$ is (13) with w_2 and w_3 having the forms (18), $\frac{\mathrm{d}w_2}{\mathrm{d}\theta} = \frac{l_1}{l_2}\frac{D_1 + D_2}{\sin^2(\theta_2 - \theta)}, \frac{\mathrm{d}w_3}{\mathrm{d}\theta} = \frac{l_1}{l_3}\frac{D_3 + D_4}{\sin^2(\theta_2 - \theta_3)}, D_i\,, i = \overline{1,4}$ have the forms (14), where θ_2=-ϕ and θ_2=ψ. Thus, the variable θ represents the solution of the nonlinear equation (23), while the variables $\phi = \phi(\theta)$ and $\psi = \psi(\theta)$ are the solutions of the system (4), where $\theta_1 = \dot{\theta}, \theta_2 = -\phi, \theta_3 = \psi, \theta_4 = 0$; the system (4) becomes:

$$f_1(\phi,\psi) = l_2\cos\phi - l_3\cos\psi + l_1\cos\theta - l_4 = 0,\ f_2(\phi,\psi) = -l_2\sin\phi - l_3\sin\psi + l_1\sin\theta = 0. \quad (24)$$

The solving of the system

To solve the system (24), a Newton-Raphson type algorithm [18] is used. Thus, starting from the approximate solution $x_0 = (\phi_0, \psi_0)$, the solution associated to the step $(k+1)$ is calculated: $\phi_{k+1} = \phi_k + \Delta\phi_k\,, \psi_{k+1} = \psi_k + \Delta\psi_k\,, k = 0,1,...,$ where $\phi_k = \phi(x_k)$, $\psi_k = \psi(x_k)$, and $\Delta x_k = (\Delta\phi_k, \Delta\psi_k)$ form the solution of the linear system:

$$I(x_k)\Delta x_k = -f(x_k), f = (f_1, f_2); \quad (25)$$

above, I is the Jacobian associated to the system (24), i.e. $I(x_k) = \begin{bmatrix} \frac{\partial f_1}{\partial \phi} & \frac{\partial f_1}{\partial \psi} \\ \frac{\partial f_2}{\partial \phi} & \frac{\partial f_2}{\partial \psi} \end{bmatrix}_{(x_k)}$. The solving of the system (25) involves the fulfillment of the condition of continuity of the partial derivatives nearness the solution $x = \lim_{k\to\infty} x_k$, as well as the fulfillment of the condition $\Delta = \det(I(x_k)) \neq 0$. The system (25) is equivalent with the following one:

$$\left(\frac{\partial f_1}{\partial \phi}\right)_{x_k} \Delta\phi_k + \left(\frac{\partial f_1}{\partial \psi}\right)_{x_k} \Delta\psi_k = -f_1(\phi_k, \psi_k), \left(\frac{\partial f_2}{\partial \phi}\right)_{x_k} \Delta\phi_k + \left(\frac{\partial f_2}{\partial \psi}\right)_{x_k} \Delta\psi_k = -f_2(\phi_k, \psi_k); \quad (26)$$

the index x_k expresses that the partial derivatives are calculated as functions of $x_k = (\phi_k, \psi_k)$. The solution of the system (26) is:

$$\Delta\phi_k = \left(-f_1 \frac{\partial f_2}{\partial \psi} + f_2 \frac{\partial f_1}{\partial \psi}\right)_{x_k} \Big/ \Delta, \Delta\psi_k = \left(-f_1 \frac{\partial f_2}{\partial \phi} + f_2 \frac{\partial f_1}{\partial \phi}\right)_{x_k} \Big/ \Delta, \Delta = \left(\frac{\partial f_1}{\partial \phi}\frac{\partial f_2}{\partial \psi} - \frac{\partial f_1}{\partial \psi}\frac{\partial f_2}{\partial \phi}\right)_{x_k}. \quad (27)$$

The functions $f_1(x_k) = f_1(\phi_k, \psi_k)$ and $f_2(x_k) = f_2(\phi_k, \psi_k)$ are expressed by means of (24), i.e. $f_1(x_k) = l_2 \cos\phi_k - l_3 \cos\psi_k + l_1 \cos\theta - l_4$, $f_2(x_k) = l_2 \sin\phi_k - l_3 \sin\psi_k + l_1 \sin\theta$.

The expressions of the partial derivatives $f_1(x_k)$ and $f_2(x_k)$ are, respectively:

$$\left(\frac{\partial f_1}{\partial \phi}\right)_{x_k} = -l_2 \sin\phi_k, \left(\frac{\partial f_1}{\partial \psi}\right)_{x_k} = l_3 \sin\psi_k, \left(\frac{\partial f_2}{\partial \phi}\right)_{x_k} = -l_2 \cos\phi_k, \left(\frac{\partial f_2}{\partial \psi}\right)_{x_k} = -l_3 \cos\psi_k. \quad (28)$$

For each value of the angle $\theta = \theta(t)$, the functions $f_1(x_k)$, $f_2(x_k)$, as well as their derivatives are determined. These are replaced in (27) and there are obtained $\Delta\phi_k$ and $\Delta\psi_k$; then, by using the equation $\phi_{k+1} = \phi_k + \Delta\phi_k, \psi_{k+1} = \psi_k + \Delta\psi_k, k = 0,1,\ldots$, one obtains $\Delta\phi_{k+1}$ and $\Delta\psi_{k+1}$. The number of iterations (k) is limited by the imposed calculation error δ. The solution is the one which verifies the error conditions $|f_1| < \delta$ and $|f_2| < \delta$. First of all, one must establish the variation limits for the angle θ and the geometric dimensions of the four-bar mechanism with respect to the beat angle ϕ range of variation. According to Fig. 3.a, for $l_3 = l_1, l_2 = \mu l_1, l_4 = \chi l_1$, the equilibrium value of the angle θ is described by equation $\cos(\theta_0) = \frac{l_4 - l_2}{2l_1} = \frac{\chi - \mu}{2}$, while, according to Figs. 3.b and 3.c, by means of the cosine's theorem, one gets:

$$\begin{aligned} \cos(\theta_1) &= \frac{(l_1 + l_2)^2 + l_4^2 - l_3^2}{2(l_1 + l_2)l_4} = \frac{(1+\mu)^2 + \chi^2 - 1}{2(1+\mu)\chi} = \frac{\mu^2 + 2\mu + \chi^2}{2(1+\mu)\chi}; \\ \cos(\theta_2) &= \frac{l_1^2 + l_4^2 - (l_2 + l_3)^2}{2l_1 l_4} = \frac{1 + \chi^2 - (1+\mu)^2}{2\chi} = \frac{\chi^2 - (\mu^2 + 2\mu)}{2\chi}. \end{aligned} \tag{29}$$

$\Delta\theta_{min} = |\Delta\theta_2|$ and $\Delta\theta_{max} = \Delta\theta_1$ express the limits (min and max) associated to variation of the angle θ with respect to the equilibrium value θ_0; the convergence of the Newton-Raphson type algorithm is conditioned by the choice of θ_0 and the value of $\Delta\theta$ which must be between $\Delta\theta_2$ and $\Delta\theta_1$. One presents below an example for the numerical calculation of the bars' rotation angles (θ, ϕ, ψ); this will be later incorporated in the block diagram of the whole control system for the automatic control of angle θ.

Numerical example

For $\mu = 0.2$ and $\chi = 0.7$, using the last expression of $\cos(\theta_0)$ and the equations (29), one gets: $\theta_0 = 75.52\,\text{deg}, \theta_1 = 56.389\,\text{deg}, \theta_2 = 87.96\,\text{deg}, \Delta\theta_1 = \theta_0 - \theta_1 = 19.13\,\text{deg}$, $\Delta\theta_2 = \theta_0 - \theta_2 = -12.44\,\text{deg}$. Thus, bar 1 oscillates from one side to another of the equilibrium position (θ_0) with $\Delta\theta \in [\Delta\theta_2 \;\; \Delta\theta_1] = [-12.44 \;\; 19.13]\text{deg}$.

For the calculation of the angles ϕ and ψ as functions of the input angle θ, the nonlinear system (24) is solved with the Newton–Raphson method, imposing:

$$\theta = \overline{\theta} = \theta_0 + \Delta\theta \sin(2\pi f t) = (75.52 + 12\sin(2\pi \cdot 100t))\deg, \tag{30}$$

error $\delta = 10^{-3}$, and the approximate initial solution $x_0 = (\phi_0, \psi_0) = (0,\ 180 - \theta_0)\deg =$ $= (0,\ 104.48)\deg$. We software implemented the above mentioned algorithm based on the Newton-Raphson method and obtained the characteristics in Fig. 4.

DESIGN OF THE SERVO-MECHANISMS' CONTROL

The automatic control of the variable ϕ (the beat angle of the insects' wing) may be indirectly achieved by means of the independent variable θ control (the rotation angle of the driving bar). The variables $\phi(\theta)$ and $\psi(\theta)$, as solutions of the nonlinear system (24), are obtained within the block 1 of the structures in Figs. 6 and 7, respectively; this is done by means of the algorithm based on the Newton - Raphson method. Also, in this section, the control of the four-bar mechanism is done, beside the usage of a proportional-derivative (PD) control law, by means of an adaptive control law based on dynamic inversion and neural networks; the control law has two components: the former is for the global nonlinearities' compensation (compensation of the dynamic inversion error), while the latter is a PD control law which is useful for the linear subsystem control with respect to the driving bar angle [19-23]. The adaptive control law design is achieved in the second sub-section of this paper's section.

Design of the control system with proportional-derivative control law

The mathematical model of the MFI's thorax is a 6 order system, having the state vector $x = [\theta \ \ \dot{\theta} \ \ \phi \ \ \dot{\phi} \ \ \psi \ \ \dot{\psi}]^T$. If the control law is proportional-derivative and it depends on θ, it will be shown that the stationary error θ_e is null and the stabilized vale of the angular rate $\dot{\theta}$ is also null; accordingly, ϕ and ψ are stabilized. Also, w_2 and w_3 are stabilized; $\dot{\phi} = -w_2\dot{\theta}$ and $\dot{\psi} = w_3\dot{\theta}$ will be stabilized to zero. Thus, we intend to prove that a PD control law with respect to θ stabilizes both the variables θ and $\dot{\theta}$, and the variables $\phi, \dot{\phi}, \psi, \dot{\psi}$.

The structure of the system for the automatic control of the angle θ with PD control law is presented in Fig. 5. The thorax's dynamics is composed of a four-bar mechanism and a piezoelectric actuator (acting on the bar 1 of the four-bar mechanism with the torque M_θ) and it is described by the nonlinear equation (23). The output of the controller is a voltage which is applied to the piezoelectric actuator.

Denoting with k_p and $k_d -$ the proportional and the derivative gains of the control law which must stabilize the MVI's flight $\left(M_\theta = k_p\theta_e + k_d\dot{\theta}_e, \theta = \bar{\theta} - \theta_e\right)$ and taking into account the form (15) for $G(\theta)$, the equation (23) becomes:

$$J(\theta)\ddot{\theta}_e + \frac{1}{2}\frac{\mathrm{d}J(\theta)}{\mathrm{d}\theta}\dot{\theta}\dot{\theta}_e + k_p\theta_e + (k_d + F(\theta))\dot{\theta}_e + \frac{1}{2}\frac{\mathrm{d}J(\theta)}{\mathrm{d}\theta}\dot{\bar{\theta}}\dot{\theta}_e = p(t), \tag{31}$$

with $p(t) = J(\theta)\ddot{\bar{\theta}} + \frac{1}{2}\frac{\mathrm{d}J(\theta)}{\mathrm{d}\theta}\dot{\bar{\theta}}^2 + F(\theta)\dot{\bar{\theta}} + G(\theta)$. We must take into consideration that $J(\theta)$, $\frac{\mathrm{d}J(\theta)}{\mathrm{d}\theta}, G(\theta)$, and $F(\theta)$ are bounded functions [10], i.e. there exist the positive constants a_1, a_2, a_3, g_1, and h_1 such that $a_1 \le J(\theta) \le a_2$, $\frac{1}{2}\left|\frac{\mathrm{d}J(\theta)}{\mathrm{d}\theta}\right| \le a_3$, $|G(\theta)| \le g_1$, $|F(\theta)| \le h_1$. Imposing that the angular rate and the angular acceleration are bounded, i.e. $\left|\dot{\bar{\theta}}\right| \le d_1$, $\left|\ddot{\bar{\theta}}\right| \le d_2$, with d_1 and $d_2 -$ positive constants, it results:

$$|p(t)| \le a_2 d_2 + a_3 d_1^2 + h d_1 + g_1. \tag{32}$$

In order to design the controller, one chooses a Lyapunov positive defined function expressing the system's total energy; it has the form [10]:

$$V(x)=V\left(\theta_e,\dot{\theta}_e\right)=\frac{1}{2}J(\theta)\dot{\theta}_e^2+\frac{1}{2}k_p\theta_e^2+\varepsilon J(\theta)\theta_e\dot{\theta}_e\,, \tag{33}$$

with $x=\left[x_1\quad x_2\right]^T=\left[\theta_e\quad \dot{\theta}_e\right]^T$ – the error vector associated to the system in Fig. 5. The Lyapunov function verifies the inequalities: $x^T Q_1 x\le V\left(\theta_e,\dot{\theta}_e\right)\le x^T Q_2 x$, where $Q_1=\frac{1}{2}\begin{bmatrix}k_p & -\varepsilon a_2\\ -\varepsilon a_2 & a_1\end{bmatrix}, Q_2=\frac{1}{2}\begin{bmatrix}k_p & \varepsilon a_2\\ \varepsilon a_2 & a_2\end{bmatrix}$. Because the Lyapunov function is positive defined, one imposes that $x^T Q_1 x$ is positive defined, i.e.:

$$\mathrm{tr}Q_1=\frac{1}{2}\left(a_1+k_p\right)>0,\det Q_1=\frac{1}{2}\left(a_1k_p-\varepsilon^2a_2^2\right)>0. \tag{34}$$

Similarly, in order that $x^T Q_2 x$ is positive defined, the following conditions must be fulfilled:

$$\mathrm{tr}Q_2=\frac{1}{2}\left(a_2+k_p\right)>0,\det Q_2=\frac{1}{2}\left(a_2k_p-\varepsilon^2a_2^2\right)>0. \tag{35}$$

Using the derivative of the function (33), by replacing $\ddot{\theta}_e$ with the form (31), and taking into account the above presented bounds of $J(\theta),\frac{\mathrm{d}J(\theta)}{\mathrm{d}\theta},G(\theta)$, and $F(\theta)$, one gets:

$$\dot{V}(x)=-x^T Q_3 x+c_1\|x\|+c_3\|x\|^3, \tag{36}$$

with $c_1=\sqrt{1+\varepsilon^2}\left(a_2d_2+a_3d_1^2+hd_1+g_1\right), c_3=\varepsilon a_3\,, Q_3=\begin{bmatrix}\varepsilon k_p & \frac{\varepsilon}{2}\left(k_d+F\right)\\ \frac{\varepsilon}{2}\left(k_d+h\right) & k_d+h-a_3d_1-\varepsilon a_2\end{bmatrix}$. The matrix Q_3 is positive defined if $\mathrm{tr}Q_3=k_d+\varepsilon k_p+h-a_3b_1-\varepsilon a_2>0,\det Q_3>0$. This matrix can be brought to the form $Q_{3d}=\begin{bmatrix}\lambda_1 & 0\\ 0 & \lambda_2\end{bmatrix}$, where λ_1 and λ_2 are the eigenvalues of the matrix Q_3, i.e. the solutions of the characteristic equation [18]:

$$\lambda^2 - \mathrm{tr}(Q_3)\lambda + \det Q_3 = 0. \tag{37}$$

The equation (36) may be put under the form: $\dot{V}(x) \le c_1\|x\| - c_2\|x\|^2 + c_3\|x\|^3$, where

$$c_2 = \min(\lambda_1, \lambda_2) = \frac{(k_d + \varepsilon k_p + h) - (a_3 d_1 + \varepsilon a_2) - \sqrt{(k_d + h - \varepsilon k_p - \varepsilon a_2)^2 + \varepsilon^2 (k_d + h)^2}}{2}. \tag{38}$$

From condition $c_2 > 0$, one gets the equation $(k_d + h)[4k_p - \varepsilon(k_d + h)] > 4a_3 d_1 (k_p + a_2)$, which differs from the one in [19]. To the last equation, one must add the second condition (34), i.e. $k_p > \varepsilon^2 a_2^2 / a_1$. Thus, the parameters of the controller (k_p and k_d) are chosen such that the following two conditions are met:

$$(k_d + h)[4k_p - \varepsilon(k_d + h)] > 4a_3 d_1 (k_p + a_2), k_p > \frac{\varepsilon^2 a_2^2}{a_1}. \tag{39}$$

Now, the last form of the function $\dot{V}(x)$ can be written as follows:

$$\dot{V}(x) = \|x\|\left(c_3\|x\|^2 - c_2\|x\| + c_1\right) = \|x\|(\|x\| - \xi_1)(\|x\| - \xi_2), \tag{40}$$

with $\xi_1 = \dfrac{c_2 - \sqrt{c_2^2 - 4c_1c_3}}{2c_3} > 0, \xi_2 = \dfrac{c_2 + \sqrt{c_2^2 - 4c_1c_3}}{2c_3} > 0; \dot{V} < 0$ if $\xi_1 < \|x\| < \xi_2$; this double inequality is verified if the conditions (39) are fullfilled.

In Fig. 6 we present the block diagram, with transfer operators, associated to the system in Fig. 5.

Design of the control system with adaptive control law

Because the dynamics of the servo-actuators (servo-mechanisms, thorax) is nonlinear and has fast time varying coefficients, the usage of PD control laws leads to dynamic processes characterized by high overshoot and angular rates, this having implications on deformation and even damage of the four-bar mechanism. Thus, in this paper, over the PD control law component, we superpose an adaptive component which must compensate the global nonlinearity (the equivalent of all nonlinearities) associated to the MFI thorax's dynamics. According to Fig. 7, the global nonlinearities may be concentrated into the function ε; this represents the h_r function approximation error (dynamic inversion error). If the control law adaptive component compensates the signal ε, then the component v_{pd} (PD type) must compensate the deviation (error) of the equivalent linear system closed by negative unitary feedback after θ, having on its direct way the linear dynamic compensator (PD type) and the linear subsystem of the MFI's dynamics with relative degree $r = 2$ with respect to the variable θ.

The dynamics of the MFI's thorax is a system with one input and one output (SISO system) described by the equations:

$$\dot{x} = f(x,u), y = h(x), \tag{41}$$

with $x = [\theta \quad \dot{\theta}]^T -$ the state vector, f and $h -$ nonlinear functions, generally unknown, $u \equiv M_\theta -$ the input, and $y = \theta -$ the output of the dynamics. System (41) satisfies the hypothesis in [22] and equations: $y^{(r)} = h_r(x,u), h_r = \dfrac{\mathrm{d}^r h}{\mathrm{d}t^r} = h^{(r)}, \dfrac{\partial h_i}{\partial u} = 0,\ 0 \le i < r; \dfrac{\partial h_r}{\partial u} \ne 0$; this means that all derivatives $y^{(i)}, 0 \le i < r$ do not depend on u, while the derivative $y^{(r)} = h_r$ depends on u; r is the relative degree of system (41). In the case of the thorax's dynamics, $r = 2$. We design a control law $\hat{v}$ after the output $y = \theta$ which has an adaptive component v_a provided by a neural network such that $y(t) \to \bar{y} = \bar{\theta}(t)$ [23]; its form is:

$$\hat{v} = \hat{h}_r(y, \hat{u}) = \hat{h}_r(\theta, \hat{M}_\theta), \tag{42}$$

where $\hat{h}_r(y,\hat{u})$ is the best approximation of the function $h_r(x,u)=h_r(x(y),u)=h_r(y,u)$. The equations $y^{(r)}=h_r(x,u), h_r=\frac{\mathrm{d}^r h}{\mathrm{d}t^r}=h^{(r)}$, and (42) are equivalent with the following ones: $u=h_r^{-1}(y,v), \hat{u}=\hat{h}_r^{-1}(y,\hat{v})$. If $\hat{h}_r\equiv h_r$ then $y^{(r)}=b_0 v\equiv b_0\hat{v}$; otherwise:

$$y^{(r)}=b_0 v, v=\hat{v}+\varepsilon, \tag{43}$$

where $\varepsilon=\varepsilon(x,u)=h_r(y,u)-\hat{h}_r(y,\hat{u})$ is the approximation error of the function h_r (the inversion error), which acts like a disturbing signal of the system. Using the Taylor series expansion of the function $u=h_r^{-1}(y,v)$ around the pair $(y,\hat{v})$, one successively obtains:

$$u=h_r^{-1}(y,v)=\hat{h}_r^{-1}(y,\hat{v})+\frac{\mathrm{d}}{\mathrm{d}v}\left(h_r^{-1}(y,v)\right)_{v=\hat{v}}=\hat{u}+\frac{\mathrm{d}}{\mathrm{d}\hat{v}}\left(\hat{h}_r^{-1}(y,\hat{v})\right)\varepsilon. \tag{44}$$

Imposing that $y\rightarrow\bar{y}$, the signal $\hat{v}$ can be chosen of form [19, 21]:

$$\hat{v}=v_{pd}-v_a+\bar{v}, \tag{45}$$

where v_{pd} is the output of the linear dynamic compensator, used for the control of the linear subsystem (43), with $\varepsilon=0, v_a -$ the adaptive command for the compensation of the error ε, while $\bar{v}$ is a robustness component of the control law which may be calculated with a formula based on the Lyapunov's theory [22]:

$$\bar{v}^T=k_z\left(\|Z\|_F+\bar{Z}\right)\|\hat{\boldsymbol{E}}\|\frac{\overline{\boldsymbol{E}}}{\|\overline{\boldsymbol{E}}\|}+k_v\overline{\boldsymbol{E}}, \tag{46}$$

with k_z and $k_v -$ positive constants (gains), $Z=\begin{bmatrix} W & 0 \\ 0 & V \end{bmatrix}; \|Z\|_F^2=\mathrm{tr}\{Z^T Z\}\le\bar{Z}$; $\|Z\|_F$ is the Frobenius norm of the matrix $Z, \bar{Z} -$ the norm of the ideal matrix associated to the neural network, $\hat{\boldsymbol{E}} -$ the estimation of the state $\boldsymbol{E}$ ($\hat{\boldsymbol{E}}$ is provided by a linear observer), $\overline{\boldsymbol{E}}=\hat{\boldsymbol{E}}^T P\bar{B}$ ($\bar{B} -$ the input matrix of the linear subsystem, $P -$ the solution of a Lyapunov equation), while W and V are the weight matrices associated to the neural network. To estimate the state vector $\boldsymbol{E}$ of the system containing the dynamic compensator and the linear subsystem (with relative degree $r=2$ and the transfer function is $H_d(\mathrm{s})=b_0/\mathrm{s}^2$), we use a linear observer described by the following equations [24]:

$$\dot{\hat{\boldsymbol{E}}}=\overline{A}\hat{\boldsymbol{E}}+L\left(\theta_e-\hat{\theta}_e\right),\hat{\theta}_e=C\hat{\boldsymbol{E}}\,, \tag{47}$$

with $\overline{A}=A-Bd_c\,, A-$ the matrix associated to the linear subsystem, $d_c=\lfloor k_p\ k_d\ 0\rfloor$, and $L-$ the gain matrix which is chosen such that the matrix $\widetilde{A}=\left(\overline{A}-LC\right)$ is asymptotically stable. The adaptive command v_a is calculated by means of a Lyapunov function $V_e\left(W,V\right)$, where $\hat{W}$ and $\hat{V}$ are the weights of the neural network *NN$_c$*; the form of the signal v_a is:

$$v_a=W^T\sigma\left(V^T\eta\right). \tag{48}$$

From the stability condition $\dot{V}_e<0$, one gets the equation system [19, 24]:

$$\dot{\hat{W}}=-\Gamma_W\left[2\left(\sigma-\sigma'\hat{V}^T\eta\right)\hat{\boldsymbol{E}}^T P\overline{B}+k\left(\hat{W}-\hat{W}_0\right)\right],\dot{\hat{V}}=-\Gamma_V\left[2\eta\hat{\boldsymbol{E}}^T P\overline{B}\sigma'+k\left(\hat{V}-\hat{V}_0\right)\right]; \tag{49}$$

in equation (49), σ is the sigmoid function $\left(\sigma(z)=\left(1+e^{-az}\right)^{-1}\right),\sigma'=\left.\dfrac{\mathrm{d}\sigma(z)}{\mathrm{d}z}\right|_{z=z_0}$ is the Jacobian of vector $\sigma,\hat{W}_0$ and $\hat{V}_0-$ the initial values of the weights $\hat{W}$ and $\hat{V}$, Γ_W,Γ_V- positive constants, $k>2\left(k_1^2+\gamma_1^2\left\|P\overline{B}\right\|^2\right),k_1=k_2\alpha_1+\left\|P\overline{B}\right\|\gamma_1\,,k_2=\left\|P\overline{B}\right\|+\left\|\widetilde{P}\overline{B}\right\|,\gamma_1\,,\alpha_1-$ positive constants, $\overline{\boldsymbol{E}}=\hat{\boldsymbol{E}}^T P\overline{B}$, while P and $\widetilde{P}(r\times r)$ are the solutions of the Lyapunov equations:

$$\overline{A}^T P+P\overline{A}=-Q,\widetilde{A}^T\widetilde{P}+\widetilde{P}\widetilde{A}=-\widetilde{Q}; \tag{50}$$

the vector $\eta[(n_1+1)\times 1]$ has the form [24]:

$$\eta=\left[1\ \hat{v}_d^T\ y_d^T\right]^T=\left[1\,I_1\ I_2\ \ldots\ I_{n1}\right]^T, \tag{51}$$

where $\hat{v}_d^T = [\hat{v}(t)\,\hat{v}(t-d)...\hat{v}(t-(n_1-r-1)d)]^T$, $y_d^T = [y(t)\,y(t-d)...y(t-(n_1-r-1)d)]^T$;

$I_1, I_2, \ldots, I_{n1}$ are the inputs of the neural network.

Separating in (23) the linear components (constants) of $J(\theta)$ and $G(\theta)$, this equation becomes:

$$\ddot{\theta} = -\frac{1}{C_0}\left(J'(\theta)\ddot{\theta} + \frac{1}{2}\frac{\mathrm{d}J(\theta)}{\mathrm{d}\theta}\dot{\theta}^2 + F(\theta)\dot{\theta} + G'(\theta) \right) + \frac{1}{C_0}(M_\theta - k\theta), \tag{52}$$

with $J'(\theta) = J(\theta) - C_0$ and $G'(\theta) = G(\theta) - (k_1 l_1^2)\theta$. Now, identifying the terms in (52) with the ones in (43), where $y = \theta$, it results:

$$\begin{aligned} &\hat{v} = \hat{h}_r(y, \hat{u}) = \hat{h}_r(\theta, \hat{M}_\theta) = -(\hat{M}_\theta - k\theta), \hat{u} = \hat{M}_\theta = \hat{h}_r^{-1}(\theta, \hat{v}) = -\hat{v} + k\theta; \\ &\varepsilon = \left(J'(\theta)\ddot{\theta} + \frac{1}{2}\frac{\mathrm{d}J(\theta)}{\mathrm{d}\theta}\dot{\theta}^2 + F(\theta)\dot{\theta} + G'(\theta) \right). \end{aligned} \tag{53}$$

ε is the approximation error which is obtained by means of the subsystem consisting of the blocks 1-6 in Fig. 6; $k = k_1 l_1^2 + k_3 l_3^2 w_3^2$. Now, taking into account (44) and the first equation (53), one yields:

$$u = M_\theta = -v + k\theta. \tag{54}$$

In stabilized regime v_a compensates the error ε such that the system in Fig. 7 is equivalent to the linear system with negative feedback after θ, having on its direct way the linear dynamic compensator and the transfer function $H_d(\mathrm{s}) = b_0/\mathrm{s}^2$, with $b_0 = -1/C_0$. For the numerical simulation of the system in Fig. 7, the two blocks (the first one connected in series with the input v and the output u, and the second one connected in series with the input u and the output θ) are replaced by the transfer function $H_d(\mathrm{s})$.

NUMERICAL SIMULATION RESULTS

Results obtained for the system with PD control law

First of all, we design the controller for the system in Fig. 5 in the case of a MAV (Micro Aerial Vehicle) insect type. The four-bar mechanism has the following parameters [3]: $m_1 = 9\,\mathrm{mg}$, $m_2^* = 2\,\mathrm{mg}$, $m_3 = 4\,\mathrm{mg}$, $m_1^* = 0.25 m_1$, $m_3^* = 0.25 m_3$, $I_2 = 4.5 \cdot 10^{-11}\,\mathrm{kg \cdot m^2}$, $l_1 = l_3 = 10\,\mathrm{mm}$, $l_2 = 2\,\mathrm{mm}$, $l_4 = 7\,\mathrm{mm}$, $l_a = 7\,\mathrm{mm}$, $k_1 = 43\,\mathrm{N/m}$, $k_3 = 6\,\mathrm{N/m}$, $b_1 = 10^{-5}\,\mathrm{Nsm}$, $b_3 = 2 \cdot 10^{-8}\,\mathrm{Nsm}$, $b_w = 9 \cdot 10^{-9}\,\mathrm{Nsm}$, $d_1 = 1\,\mathrm{rad/s}$, $d_2 = 1\,\mathrm{rad/s^2}$. By using the calculation equations presented in the previous sections, we determine the variation domains of all the coefficients; one yields: $w_2 \in (20, 40), w_3 \in (1, 10), D_1 \in (0, 0.8), D_2 \in (0.8, 1.4), D_3 \in (1, 20), D_4 \in (1.7, 21)$; $\left(\frac{\mathrm{d}w_2}{\mathrm{d}\theta}\right)_{\max} = 3 \cdot 10^4\,\mathrm{rad^{-1}}, \left(\frac{\mathrm{d}w_3}{\mathrm{d}\theta}\right)_{\max} = 2.3 \cdot 10^3\,\mathrm{rad^{-1}}$. With these, we obtained: $a_1 = 4 \cdot 10^{-7}\,\mathrm{kg \cdot m^2}$, $a_2 = 2 \cdot 10^{-7}\,\mathrm{kg \cdot m^2}$, $a_3 = 7 \cdot 10^{-4}\,\mathrm{kg \cdot m^2/rad}$, $g_1 = 1.5 \cdot 10^{-2}\,\mathrm{Nm}$, $h = 1.5 \cdot 10^{-5}\,\mathrm{Nsm/rad}$. Choosing $\varepsilon = 0.5$, we also obtained the controller's gains: $k_p = 120$, $k_d = 8 \cdot 10^{-4}\,\mathrm{s}$. We have software implemented the system in Fig. 6 and we obtained the characteristics in Figs. 8 and 9. For the software implementation of the Newton-Raphson algorithm, we used the Matlab function "*embedded*" which requests the existence of a C compiler; this compiler works together with the toolbox of the Matlab/Simulink. In Fig. 8 we presented the time charteristics of the system in Fig. 6 for a step type input having the form: $\overline{\theta}(t) = \theta_0 + \Delta\theta \cdot 1(t) = (75.52 + 12 \cdot 1(t))\,\mathrm{deg}$. The system has an overshoot and the signal θ is stabilized to the value 87.52 deg. in a very short time $(10^{-4}\,\mathrm{s} = 10^{-2} T, T = 1/f)$, with null stationary error, while the signals θ and ψ are stabilized too; $\dot{\theta}$ is stabilized to zero.

The non-dimensional variables w_2 and w_3 are also stabilized and, accordingly, $\dot{\phi}$ and $\dot{\psi}$ become null. The form of the time characteristic $\dot{\theta}(\theta)$ (which is called the portrait phase) expresses the absolute stability of the nonlinear system in Fig. 6; the characteristic leads to a stable limit cycle.

For a sinusoidal type input $\overline{\theta} = \theta_0 + \Delta\theta \sin(2\pi f t) = (75.52 + 12\sin(2\pi 100 t))\deg$, we obtained the characteristics in Fig. 9. The system follows very closely the input signal and has null stationary error. The variables w_2 and w_3 are stabilized; $\dot{\theta}$ and, accordingly, $\dot{\phi}$ and $\dot{\psi}$ are stabilized at high values.

Results obtained for the system with adaptive control law

For the system in Fig. 7, using the same parameters like the ones associated to Fig. 6, we calculate the gains (parameters) of the dynamic compensator k_p and k_d such that the roots of the characteristic equation:

$$\mathrm{s}^2 + b_0 k_d \mathrm{s} + b_0 k_p = 0 \tag{55}$$

are situated in the left-side complex plane. Thus, imposing for this characteristic equation, for example, the roots: -380 and -480, we obtained $k_p = -7.75 \cdot 10^{-5}$ and $k_d = -3.65 \cdot 10^{-7}$. The linear observer is described by the equation (47); $\hat{\boldsymbol{E}}$ is the estimation of the state $\boldsymbol{E} \equiv \boldsymbol{e} = [\theta_e \; \dot{\theta}_e]^T$. The observer gain matrix L is chosen such that the matrix $\tilde{A} = \overline{A} - L\overline{C} = \overline{A} - LC = \overline{A} - Lc$ is stable (desired eigenvalues are imposed for the matrix $\tilde{A}$); we have used $A = \begin{bmatrix} 0 & 1 \\ 0 & 0 \end{bmatrix}, \overline{B} = B = \begin{bmatrix} 0 \\ b_0 \end{bmatrix}, c = [1 \;\; 0]^T, \overline{A} = A - Bd_c,\; d_c = [k_p \;\; k_d]$. By using as eigenvalues for $\tilde{A}$ the negative constants -380 and -480, we obtained the gain matrix $L = 10^{-7}[0.832 \quad 0.0039]^T$. The matrix P (the solution of the first equation (50)), using $Q = 0.2 I_2$ (I_2 – the identity matrix), is $P = \begin{bmatrix} 21.209 & 0 \\ 0 & 0.0001 \end{bmatrix}$. The matrices W and V are calculated with (49), by using the constants $\Gamma_w = \Gamma_v = 0.05$. The robustness component of the adaptive control law $\bar{v}$ is obtained by means of (46) where $k_z = 0.01, k_v = 0.001, \bar{Z} = 1$. For the neural network, we chosen $n_1 = 9$ input neurons, $n_2 = 10$ neurons in the hidden layer and $n_3 = 1$ output neuron. In this case, the input vector is: $\eta = [1 \; \hat{v}(t) \; \hat{v}(t-d) \; y(t) \; y(t-d \ldots y(t-6d))]^T$ with $d = 0.001$. The vector a appearing in the expression of the sigmoid function $\left(\sigma(z) = \left(1 + e^{-az}\right)^{-1}\right)$, is the so-called neural network activation potentials' vector; for this example, it has been chosen as: $a = [1 \quad 0.9 \quad 0.8 \quad 0.7 \quad 0.6 \quad 0.5 \quad 0.4 \quad 0.3 \quad 0.2 \quad 0.1]$.

In Fig. 10 we present the Matlab/Simulink model of the system in Fig. 7; it has many subsystems and represents the software implementation of the block diagram in Fig. 7 – the adaptive system for the control of the MFI's thorax; by means of this Matlab/Simulink model and a software program in Matlab environment, we have obtained the time characteristics in Figs. 11 and 12 associated to the system with step input type and sinusoidal input type, respectively. The form of the time characteristics $\dot{\theta}(\theta)$ expresses the absolute stability of the nonlinear system in Fig. 7; this characteristic leads to a stable limit cycles. When the input is a step type signal, θ and, accordingly, ϕ and ψ are stabilized with null stationary error; w_2 and w_3 are also stabilized, while $\dot{\theta}, \dot{\phi}$, and $\dot{\psi}$ become null. Comparing the responses of the two systems for a step type input (see the characteristics in Figs. 8 and 11), we remark that the characteristics in Fig. 8 (for a PD control law) are faster and have overshoot, while the characteristics in Fig. 11 (adaptive control law) are not characterized by overshoot; the stationary errors are null for both systems. For a sinusoidal type input, the response of the adaptive control system reproduces the input signal (as form), but it is characterized by a small delay with respect to the input signal; the response of the system having PD control law also reproduces the input signal.

CONCLUSIONS

In this paper we deduced nonlinear forms of the dynamic models for the deformable and non-deformable four-bar mechanisms (three bars are mobile, while one bar is fixed). The dynamic model of the four-bar mechanism is a six order system; the state variables are the angles and the angular rates of the bars $\left(\theta, \phi, \psi, \dot{\theta}, \dot{\phi}, \dot{\psi}\right)$. The variables ϕ, ψ (which depend on the independent variable θ) have been calculated by using a Newton-Raphson type algorithm. For the choice of the initial approximate solution $\left(\phi_0, \psi_0\right)$, to ensure the convergence conditions, we established the variation limits for the independent variable and the geometric dimensions of the four-bar mechanism with respect to the range of variation of the wing beat angle (ϕ). The angular rates $\dot{\phi}$ and $\dot{\psi}$ have been obtained with respect to $\dot{\theta}$ and the transmission ratios $w_2(\theta, \phi, \psi)$ and $w_3(\theta, \phi, \psi)$. The control of the four-bar mechanism has been achieved directly by means of the control of the variables $\theta, \dot{\theta}$ using a PD control law; the parameters of this control law have been obtained by means of a Lyapunov function. Indirectly, the control of the other states $\left(\phi, \dot{\phi}, \psi, \dot{\psi}\right)$ has been also accomplished. To decrease the overshoots and, thus, the possible damage of the four-bar mechanism, we designed an adaptive control law based on the dynamic inversion and neural networks. The validation of the theoretical results (two control systems) has been achieved by means of complex numerical simulations; these are very good and they have been analyzed in the fourth section of the paper.

REFERENCES

[1] Avadhanula, S., Wood, R. J., Campolo, D., Fearing, R. S., 2002, "Dynamically Tuned Design of the MFI Thorax," Proceedings of the 2002 IEEE International Conference on Robotics and Automation, Washington, USA, pp. 52-59.

[2] Zhang, W., Li, Q., Guo, L., 1999, "Integrated Design of Mechanical Structure and Control Algorithm for a Programmable Four Bare Linkage," IEEE/ASME Transactions on Mechatronics, **4**(1), pp. 354-362.

[3] Sitti, M., 2003, "Piezoelectrically Actuated Four-Bar Mechanism with Two Flexible Links for Micromechanical Flying Insect Thorax," IEEE/ASME Transactions on Mechatronics, **8**(1), pp. 26-36.

[4] Sitti, M., 2001," PZT Actuated Four Bar Mechanism with Two Flexible Links for Micromechanical Flying Insects Thorax," Proceedings of the IEEE International Conference on Robotics and Automation, Korea, pp. 3893-3900.

[5] Sitti, M., Campolo, D., Yan, J., Fearing, R. S., 2001, "Development of PZD and PZN – PT Based Unimorph Actuators for Micromechanical Flapping Mechanism," Proceedings of the IEEE International Conference on Robotics and Automation, pp. 3839-3846, Korea.

[6] Wang, Q., Zhang, B. X, Liu, R., Cross, L., 1999," Nonlinear Piezoelectric Behavior of Ceramic Bending Mode Actuators under Strong Electric Fields," Journal of Applied Physics, **86**(6), pp. 3352-3360.

[7] Wang, Q., Du, X., Xu, B., Cross, L., 1999, "Electromechanical Coupling and Output Efficiency of Piezoelectric Bending Actuators," IEEE Transactions on Ultrasonic, Ferroelectrics and Frequency Control, **46**(3), pp. 638-646.

[8] Yan, J., Dikinson, M., Sitti, M., Su, T., Fearing, R. S., 2002, "Wing Transmission for a Micromechanical Flying Insect," Journal of Micromechatronics, **1**(3), pp. 221-237.

[9] Bidakhvidi, M. A., Vanlanduit, S., Shirzadeh, R., Vucinic, D., 2012, "Experimental and Computational Analysis of the flow Induced by a Piezoelectric Fan," Proceedings of the 15th International Symposium on Flow Visualization, Minsk, Belarus.

[10] Wu, F. X., Zhang, W. J., Li, Q., Oniang, P. R., 2002, "Integrated Design and PD Control of High-Speed Closed-loop Mechanisms," Journal of Dynamic Systems, Measurement and Control, **124**, pp. 522-528.

[11] Fearing, R., Chiang, K., Dickinson, M., Pick, D., Sitti, M., Yan, I., 2000, "Transmission Mechanism for Micromechanical Flying Insects," Proceedings of the IEEE International Conference on Robotics and Automation, SUA, San Francisco, pp. 1509-1516.

[12] Hines, L., Campolo, D., Sitti, M., 2013, “Liftoff of a Motor-driven Flapping Wing Micro aerial Vehicle Capable of Resonance,” IEEE Transactions on Robotics, **PP**(99), pp. 1-13, DOI: 10.1109/TRO.2013.2280057.

[13] Hines, L., Arahagi, V., Sitti, M., 2012, “Shape Memory Polymer - Based Flexure Stiffness Control in Miniature Flapping-Wing Robot,” IEEE Transactions on Robotics, **28**(4), pp. 987-990.

[14] Sahai, R., Galloway, K. C., Wood, R. J., 2013, “Elastic Element Integration for Improved Flapping – Wing Micro Air Vehicle Performance,” IEEE Transactions on Robotics, **29**(1), pp. 32-41.

[15] Arahagi, V., Hines, L., Sitti, M., 2013, “A Simulation and Design Tool for a Passive Rotation Flapping wing Mechanism,” IEEE Transactions on Robotics, **18**(2), pp. 787-798.

[16] Shimozama, I., Miura, H., Suzuki, K., Ezura, Y., 1993, “Insect – like Micro robots with External Skeletons,” IEEE Control Systems Magazine, **13**(1), pp. 37-41.

[17] Demian, T., 1970, *Mecanisme şi elemente constructive de mecanică fină.* Didactic and Pedagogic Publisher, Bucharest.

[18] R. Lungu, 2000, *Automatizarea aparatelor de zbor (Flight aparatus automation)*, Universitaria Publisher.

[19] Calise, A. J, Hovakymyan, N., Idan, M., 2001, ”Adaptive Output Control of Nonlinear Systems Using Neural Networks,” Automatica, **37**(8), pp. 1201-1211.

[20] Chwa, D., Choi, J., 2003, “Adaptive Nonlinear Guidance Law Considering Control Loop Dynamics,” IEEE Transactions on Aerospace and Electronic Systems, **39**(4), pp. 134-1143.

[21] Gregory, L. P., 1998, *Adaptive Inverse Control of Plants with Disturbances*, Stanford University.

[22] Isidori, A., 1995, *Nonlinear Control Systems*, Springer, Berlin.

[23] M. Lungu, 2008, *Sisteme de conducere a zborului (Flight control systems)*, Sitech Publisher.

[24] Lungu, R., Lungu, M., Rotaru, C., 2011, “Non-linear adaptive system for the control of the helicopters pitch’s angle,” *Proceedings of the Romanian Academy, Series A: Mathematics, Physics, Technical Sciences, Information Science*, **12**(2), pp. 133-142.

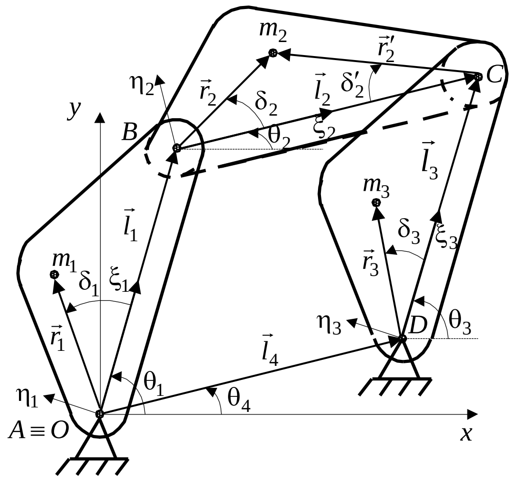

Fig. 1 The four-bar mechanism

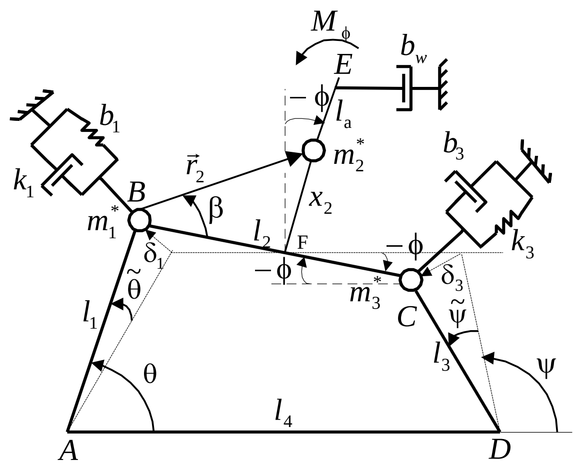

Fig. 2 The mechanical model associated to the mechanism with four elastic bars

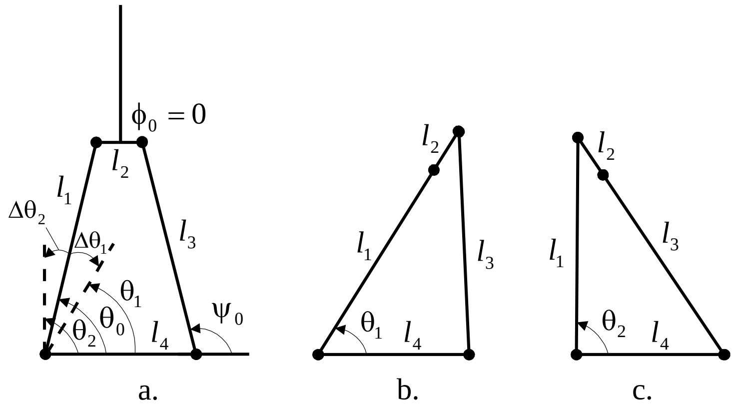

Fig. 3 The neutral and the extreme orientation positions of the mechanism’s bars

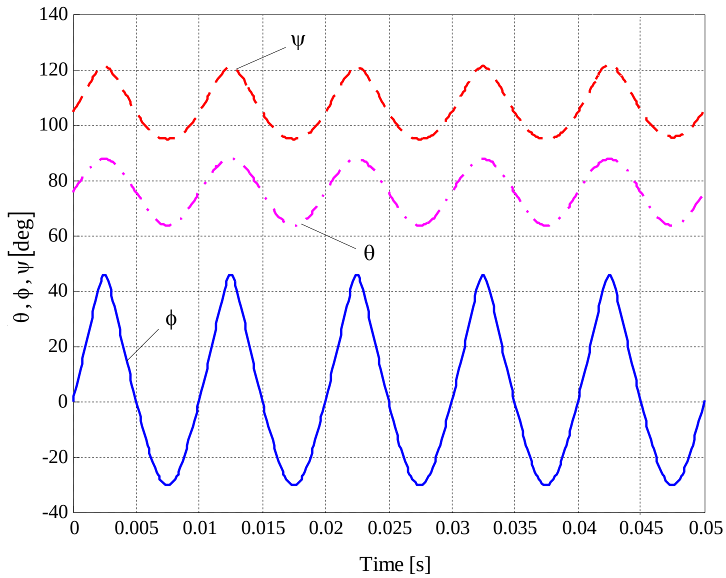

Fig. 4 Time histories $\theta(t), \phi(t), \psi(t)$

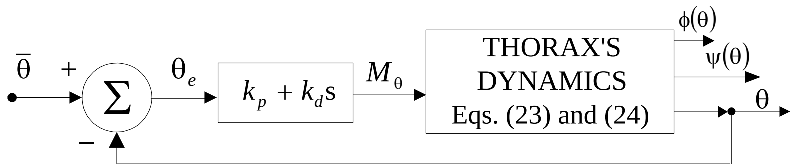

Fig. 5 Structure of the system for the automatic control of angle θ, with PD control law

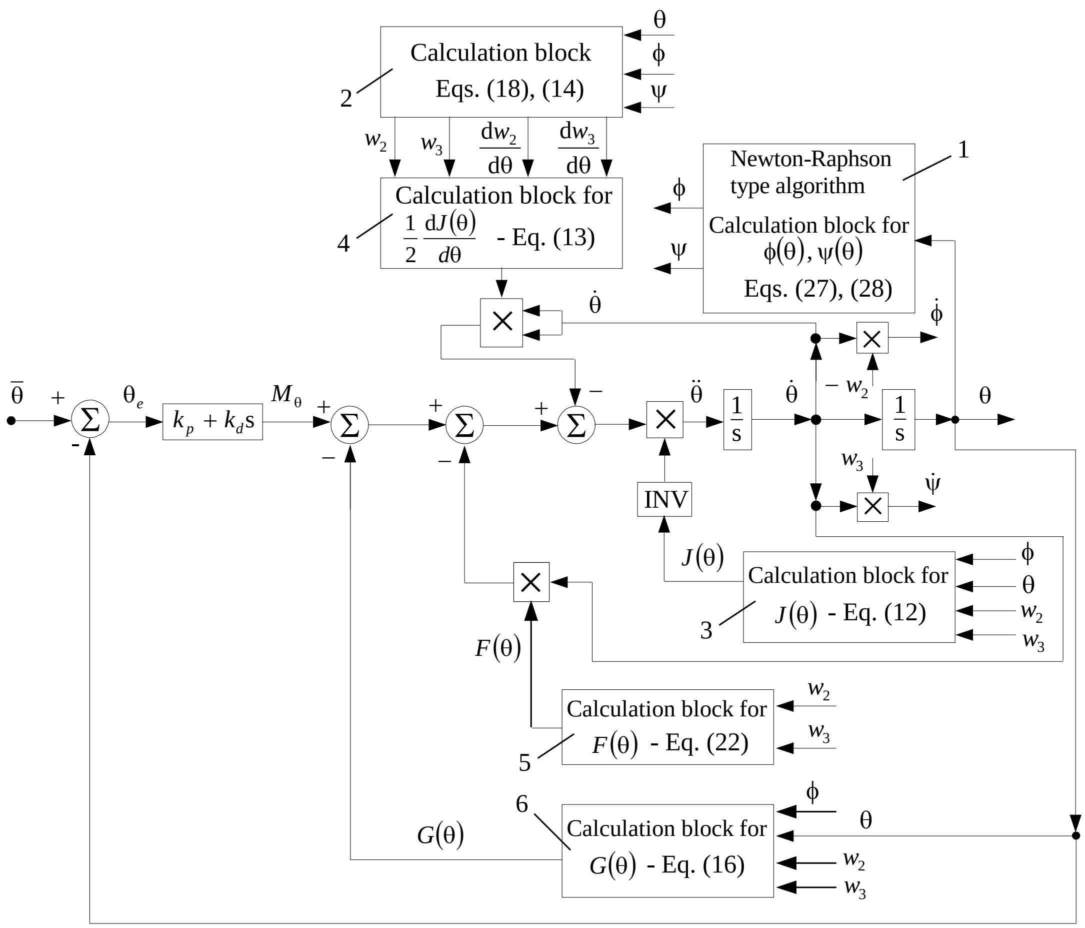

Fig. 6 The block diagram, with transfer operators, associated to the system in Fig. 5

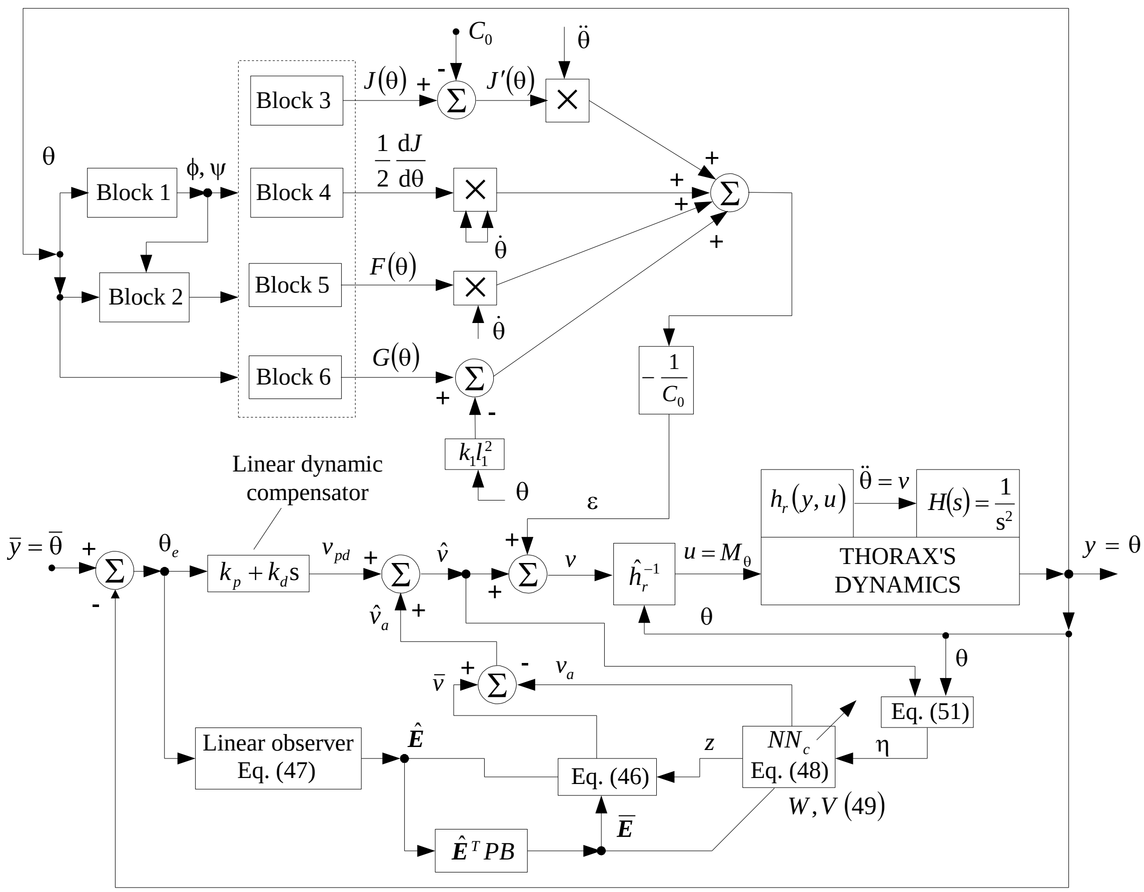

Fig. 7 The adaptive system for the control of the MFI's thorax

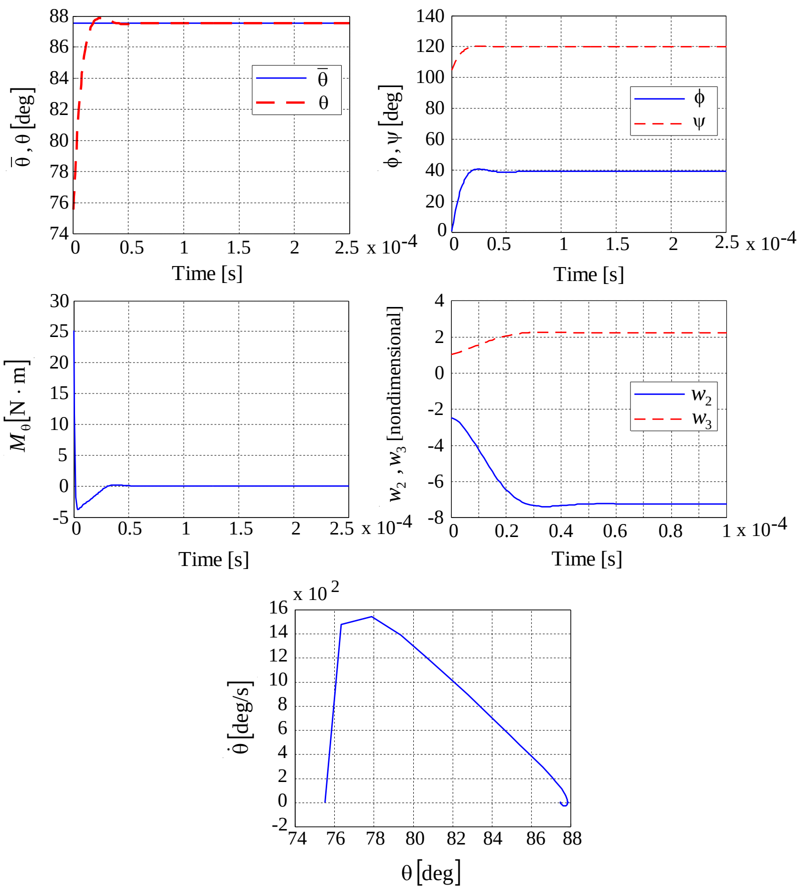

Fig. 8 The characteristics obtained for the system in Fig. 6 for a step type input

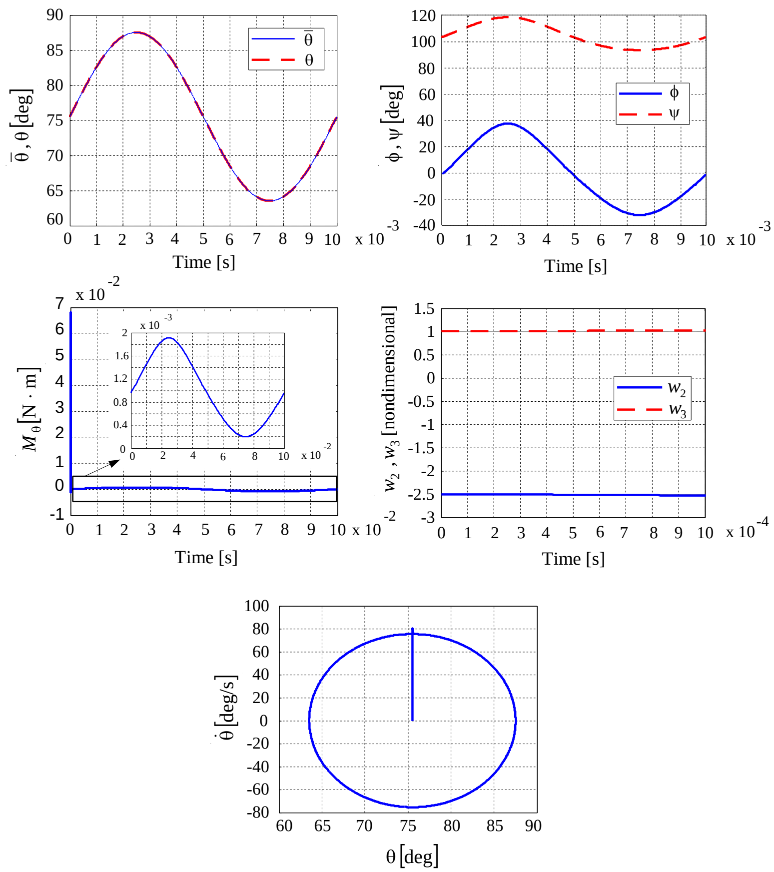

Fig. 9 The characteristics obtained for the system in Fig. 6 for a sinusoidal type input

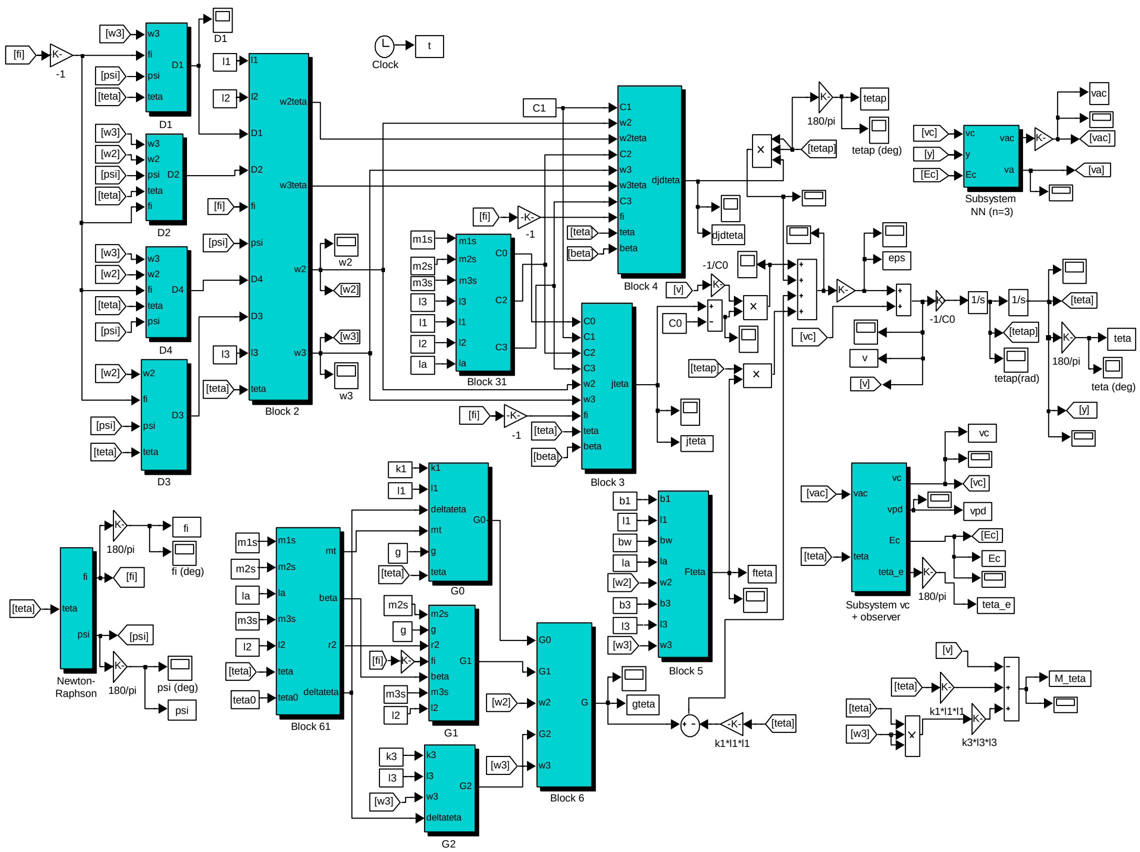

Fig. 10 Matlab/Simulink model of the system in Fig. 7

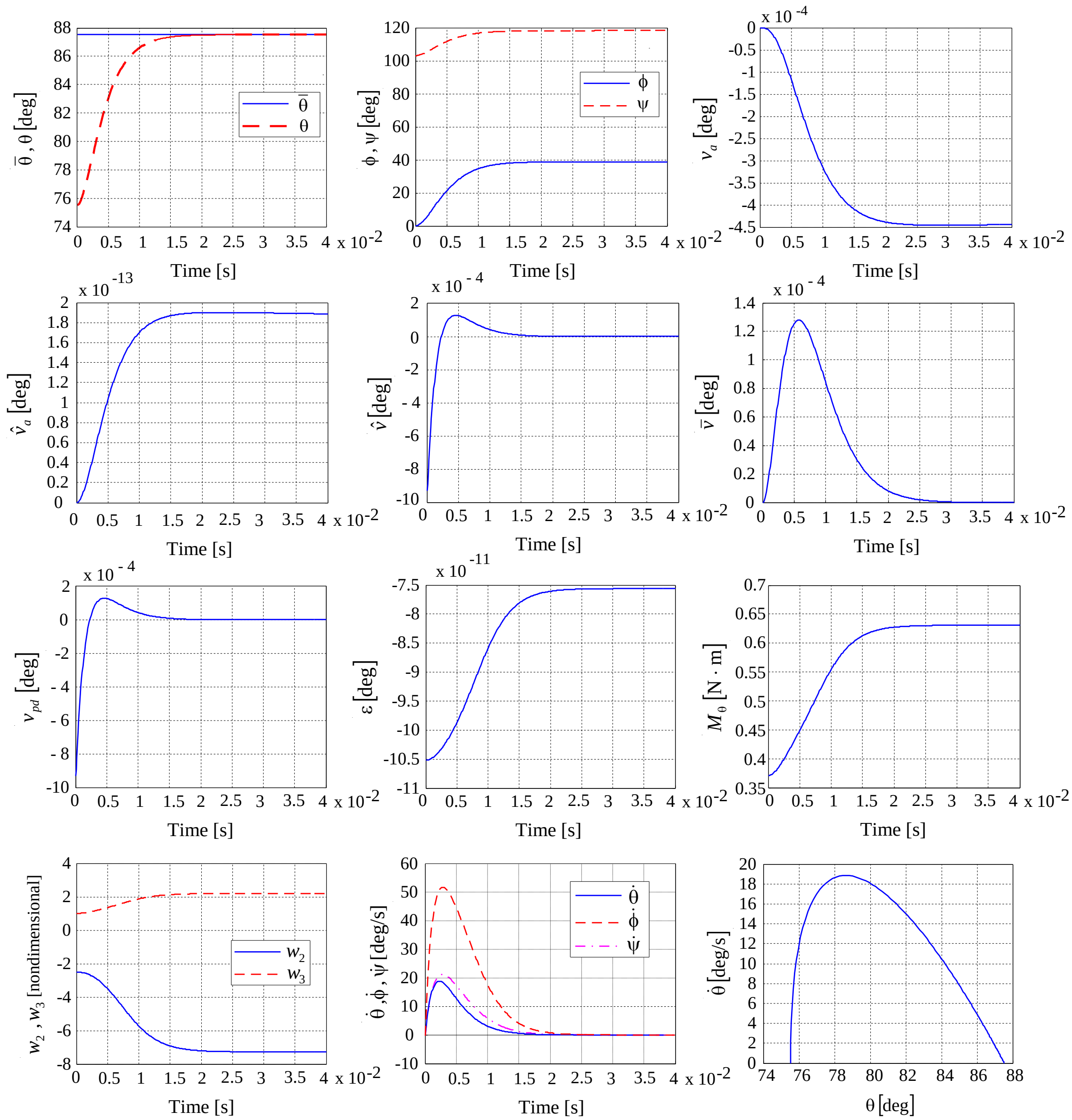

Fig. 11 The characteristics obtained for the system in Fig. 7 for a step type input

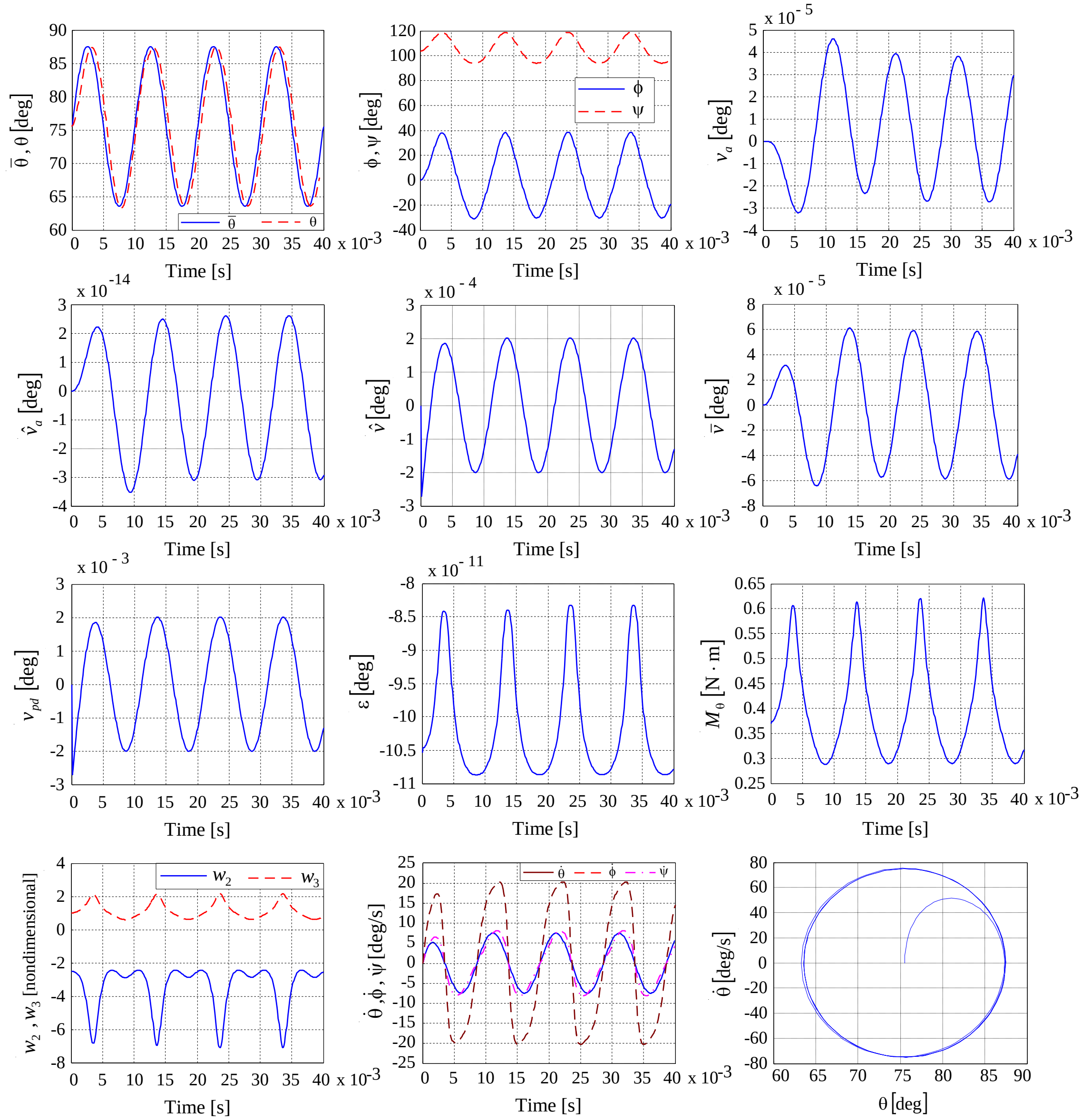

Fig. 12 The characteristics obtained for the system in Fig. 7 for a sinusoidal type input